Behaviour of slender square concrete-filled stainless steel columns subject to axial load

B. Uy[1], Z. Tao[1,2], F. Y. Liao[3] & L. H. Han[3]
[1]*School of Engineering, University of Western Sydney, Sydney, Australia*
[2]*College of Civil Engineering, Fuzhou University, Fuzhou, China*
[3]*Department of Civil Engineering, Tsinghua University, Beijing, China*

ABSTRACT: Due to its excellent corrosion resistance, decorative qualities, ease of maintenance and fire resistance, the past few decades have seen the accelerating interest in the use of stainless steel in construction throughout the world. Concrete-filled steel tubular columns comprised of stainless steel ideally combines the advantages of both stainless steel and concrete. So far, research on the concrete-filled stainless steel tubular (CFSST) columns is still quite limited, and mainly focused on short columns. In practice, columns are usually subjected to the influence of slenderness. A total of 6 square CFSST columns were tested under axial loading conditions to evaluate the influence of global slenderness. Several existing design codes, including the Australian design code AS 5100 (2004), American code AISC (2005), Chinese code DBJ 13-51-2003 (2003) and Eurocode 4 (2004), are used to predict the column strength and are compared with the test results. This is helpful in evaluating the applicability of the current codes in calculating the strength of slender CFSST columns.

1 INTRODUCTION

Concrete-filled stainless steel tubular (CFSST) columns are considered promising for their use in structural applications. So far, research on CFSST columns is still quite limited, and the past studies have mainly concentrated on the behaviour of stub columns (Young & Ellobody, 2006, Lam & Gardner, 2008, Uy, 2008). A literature review has shown that there is no research work conducted on slender CFSST columns. In practice, columns are usually subjected to the influence of slenderness, and a slenderness reduction factor in this case should be applied for design purposes. Against the above background, tests on 6 square composite columns were conducted recently with an aim to investigate the performance of slender CFSST columns. Several existing design codes, including the Australian design code AS 5100 (Standards Australia, 2004), American code AISC (American Institute of Steel Construction, 2005), Chinese code DBJ 13-51-2003 (2003) and Eurocode 4 (2004), are used to predict the column strength and compare with the test results. These codes are to be referred to as “AS 5100”, “AISC”, “DBJ” and “EC4” in the following.

2 EXPERIMENTAL PROGRAM

2.1 *General*

Six tests were planned as shown in Table 1, in which concrete cylinder strength f_c' (36.3, 75.4 MPa) and slenderness ratio λ (15.2-87.7) were selected as the investigating parameters. In order to distin-

guish specimens with different parameters, the specimen labels are assigned according to (1) section shape (S1 represents specimen with square section); (2) slenderness ratio (1, 2 and 3 used to distinguish specimens with different slenderness ratios); and (3) concrete strength ("a" for normal strength concrete and "b" for high strength concrete). Slenderness ratio (λ) is defined as

$$\lambda = 2\sqrt{3}L_e / B \quad (1)$$

where L_e is the effective length of a column, and B is the overall sectional width.

Table 1. Details of specimens and test results

No.	Specimen label	$B\times t$ (mm)	Length L_e (mm)	λ	$\sigma_{0.2}$ (MPa)	f_c' (MPa)	N_{ue} (kN)	$u_{m,ult}$ (mm)	ε_{cu} (με)	ε_L (με)
1	S1-1a	100.3×2.76	440	15.2	390.3	36.3	767.6	0.33	9102	5778
2	S1-1b	100.3×2.76	440	15.2	390.3	75.4	1090.5	0.29	3846	2162
3	S1-2a	100.3×2.76	1340	46.3	390.3	36.3	697.3	2.65	4383	2465
4	S1-2b	100.3×2.76	1340	46.3	390.3	75.4	1022.9	0.83	3040	1557
5	S1-3a	100.3×2.76	2540	87.7	390.3	36.3	622.9	4.42	2451	1773
6	S1-3b	100.3×2.76	2540	87.7	390.3	75.4	684.2	10.82	2423	1050

2.2 *Material properties*

All specimens were fabricated from cold-formed tubes with a measured width (B) and thickness (t) of 100.3 mm and 2.76 mm, respectively. The internal radius of the rounded corners was 1.8 mm for all tubes. Tensile coupons extracted from the flat surfaces of a tube were conducted to measure the material properties of the stainless steel. The three basic Ramberg-Osgood parameters, i.e., the initial elastic modulus E_0, the 0.2% proof stress $\sigma_{0.2}$, and the strain-hardening exponent n, are 182 GPa, 390.3 MPa and 6.7, respectively. Two types of concrete, with the cylinder compressive strength (f_c') at 28 days of 30.2 MPa and 58.6 MPa, respectively, were used to fill the hollow sections. The achieved average compressive strengths at the time of testing were 36.3 MPa and 75.4 MPa, respectively. The corresponding moduli of elasticity (E_c) were 33900 MPa and 37900 MPa, respectively.

2.3 *Specimen preparation*

Cold-formed hollow stainless steel sections were cut according to their required dimensions. A steel end plate with a thickness of 15 mm was welded to the bottom end of each tube before filling the tube with concrete. Commercial concrete was ordered and delivered to the laboratory. The concrete was filled in layers and a poker vibrator was used for compaction requirements. The specimens were placed upright to air-dry until testing. During curing, a very small amount of longitudinal shrinkage occurred at the top of the columns. Prior to the welding of the top plate, high-strength mortar was used to fill the gap so that the concrete surface was flush with the stainless steel tube at the top. In order to avoid the occurrence of local failure at the specimen ends, four steel stiffeners with a height of 50 mm were welded to each end of the column, as shown in Figure 1.

2.4 *Instrumentation and loading setup*

All the axial loading tests were undertaken using a 3000 kN capacity Instron testing machine. In order to simulate pin-ended supports, two spherical hinges with a diameter of 140 mm were installed at both ends of each column before testing, as shown in Figure 1. The instrumentation used during the tests includes both load-lateral deflection as well as strain readings. Six linear variable displacement transducers (LVDT) were used to measure the out-of-plane deflections of a column at two perpendicular directions along the specimen height. Owing to the limited installation space, deflections were only measured at the mid-height for the two shortest specimens S1-1a and S1-1b. Eight strain gauges with a gauge length of 3 mm were used for each specimen to measure the longitudinal and transverse strains at the mid-height, as shown in Figure 1. Displacement control was used for the loading with a rate of 0.2 mm/min before the peak load was reached. After that, the loading rate was set to be 0.6 mm/min.

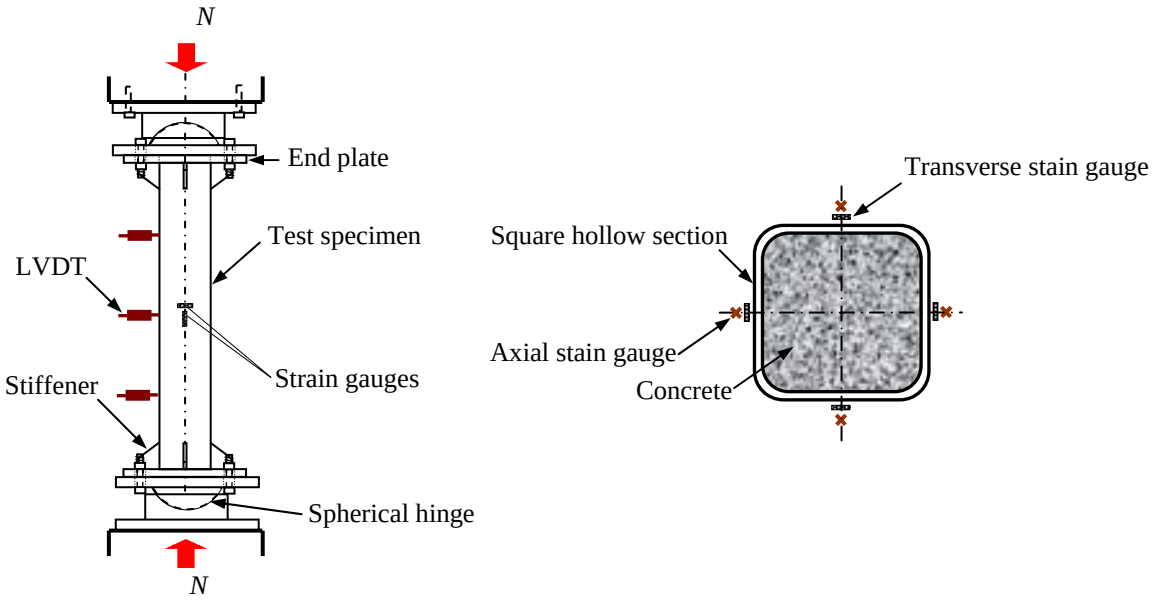

Figure 1. Test setup.

3 TEST RESULTS AND DISCUSSIONS

3.1 *Test observations*

The test results of the columns are summarised in Table 1, where $u_{m,ult}$ is the mid-height deflection at peak load (N_{ue}), ε_{cu} and ε_L are the axial and lateral strains at peak load, which were measured from the strain gauges located at the extreme compression fibre. Figure 2 shows a general view of typical specimen after testing. It was observed that all long columns failed in a typical flexural mode with large lateral deflections, as shown in Figure 2. For the two shortest columns, i.e., S1-1a and S1-1b, their failure was characterised by axial compression. Despite this, obvious bending deformation has also developed at the end of the testing. Since the utilised square hollow section was compact, local buckling was only observed after the peak load had been attained. The local buckling of steel tubes occurred generally near the specimen mid-height, as shown in Figure 2.

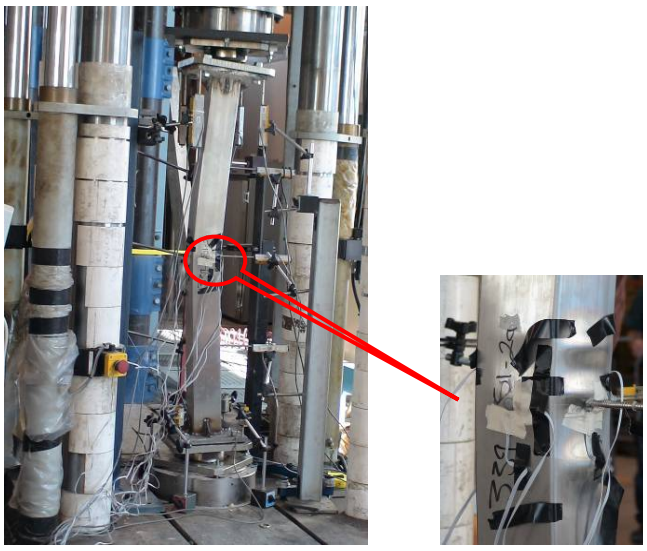

Figure 2. A general view of typical specimen after testing.

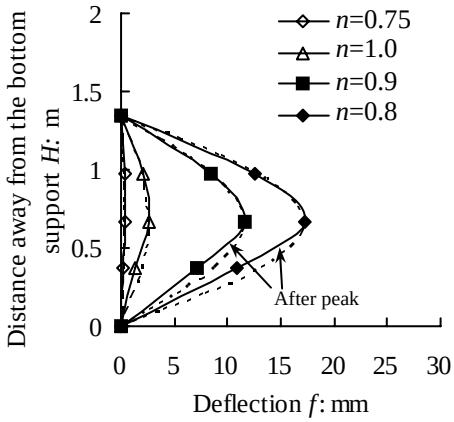

Figure 3. Column deflection development.

Lateral deflections were measured along the column height for specimens with an L_e of 1340 mm or 2540 mm. As expected, the lateral deformation was not obvious before the peak load was reached.

The strain readings indicated that the column was under nearly axial compression. After that, the lateral deformation developed progressively accompanied by load reduction. For a longer column, obvious lateral deformation was generally observed in the two perpendicular directions for measurement, whilst a shorter column bent predominantly in one direction. At the initial loading stage, generally, the deflection curves of a specimen were not completely symmetrical owing to the random distribution of initial global imperfections. During the post-peak stage, the deflection curves were approximately in the shape of half-sine wave. This observation is illustrated in Figure 3 with the typical specimen S1-2a, where the deflections of the column are the combination of the measurements in two directions, and compared with corresponding sine curves shown as dashed lines for different levels of axial loads before and after failure. The axial load levels are represented by the axial load ratio n which is defined as the ratio of the applied load N to the peak load N_{ue}. From the above test observations, it seems that there is no obvious difference between CFSST columns and conventional concrete-filled steel tubular (CFST) columns fabricated from carbon steel in terms of test observation and failure mode (Han, 2000).

3.2 *Effect of slenderness ratio*

The effect of slenderness ratio (λ) on the axial load (N) versus mid-height lateral deflection (u_m) curves is shown in Figure 4. As can be seen, the larger the slenderness ratio, the smaller the peak load is. Also, the post-peak curves become steeper with decreasing λ. According to EC4, the shortest columns have attained their section capacities, whilst the two longest columns S1-3a and S1-3b only attained 83% and 62% of their section capacities, respectively. It is thus expected that slenderness reduction factors should be applied in designing slender CFSST columns.

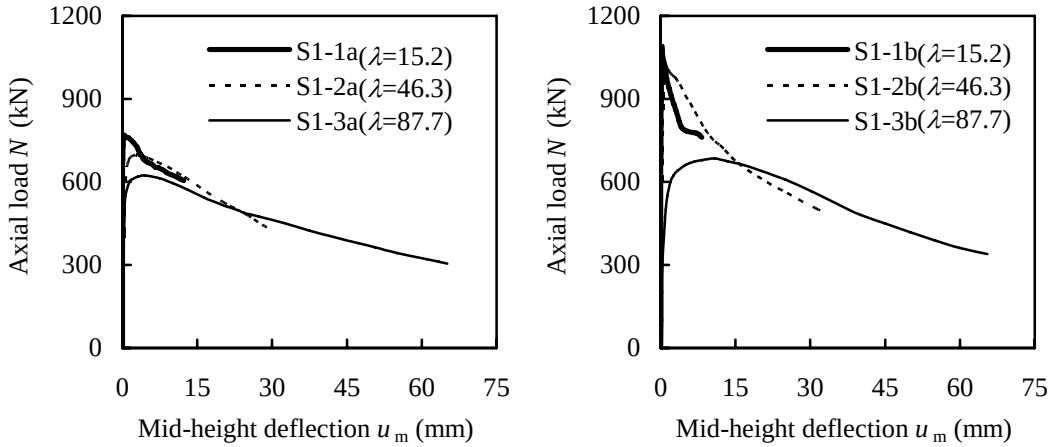

Figure 4. Effect of slenderness ratio on N-u_m curves.

Figure 5 demonstrates the effect of slenderness ratio on the N-Δ/L curves, where Δ is the measured axial shortening, and L is the length of a column. As can be seen, the initial portion of the N-Δ/L curve for a longer column essentially followed the curve of its corresponding shorter column before attaining the peak load. It can also be seen from Figure 5 that, the larger the slenderness ratio, the smaller the value of Δ/L at the peak load is. This trend is more obvious for these columns in-filled with high-strength concrete. Owing to the influence of global slenderness, only the shortest columns have developed Δ/L at the peak loads with values bigger or near the steel yield strain (4145 με), as shown in Figure 5.

3.3 *Effect of concrete strength*

The effect of concrete strength on the N-u_m curves is depicted in Figure 6. It can be seen that more ductile behavior was achieved as normal strength concrete was used. This trend is less obvious with the increase of slenderness ratio, owing to the fact that slender columns generally undergo elastic buckling.

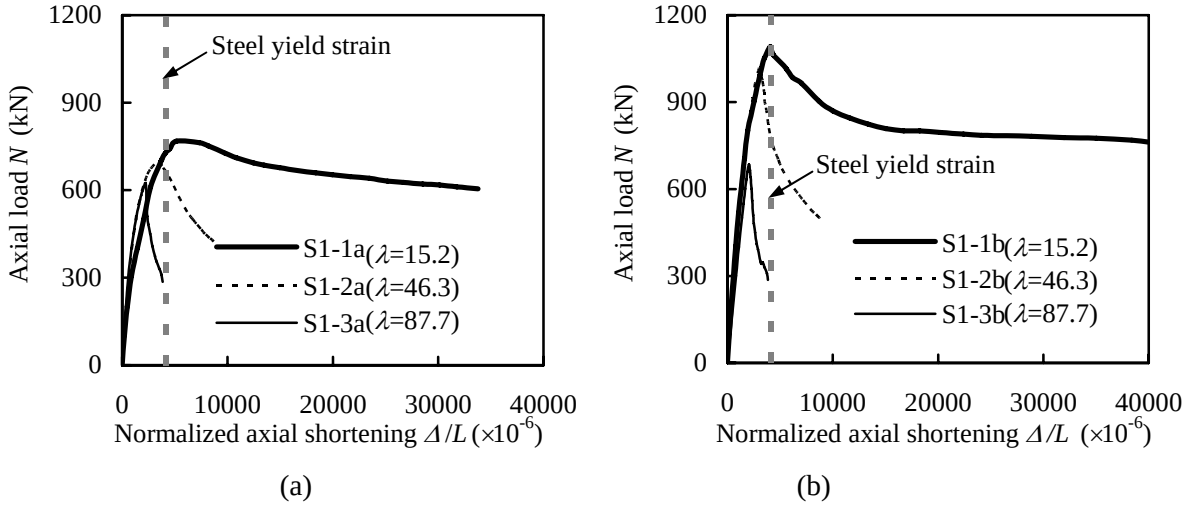

(a) (b)

Figure 5. Effect of slenderness ratio on N-Δ/L curves.

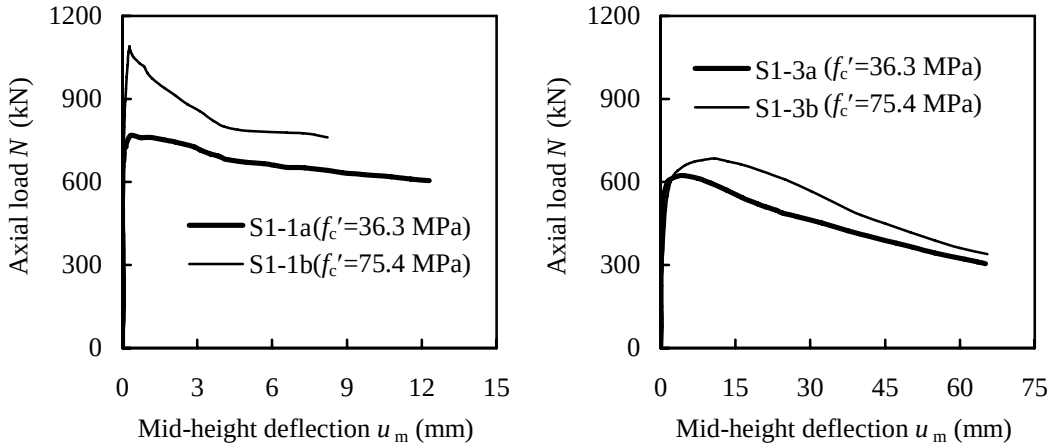

(a) (b)

Figure 6. Effect of concrete strength on N-u_m curves.

3.4 *Strain analysis*

Figure 7 shows the axial and lateral strain development for two typical specimens S1-1a and S1-3b, where the strains were measured at the column mid-height. The strain readings from strain gauges located on four different tube surfaces are all shown in Figure 7. As can be seen, the whole section for each column was under compression before the peak load was reached. During this stage, there was no obviously difference among the measured strains at different locations. This demonstrated that the column was under nearly uniform compression. After the peak load was reached, part of the cross-section for a longer column reversed from compression to tension, as shown in Figure 7(b). This is due to the more prominent second-order effect resulting in the generation of excess second-order moment. The effect of slenderness ratio and concrete strength on the ultimate strain (ε_{cu}) is shown in Figure 8. It is observed from Figure 8 that the value of ε_{cu} decreases with the increase of slenderness ratio. This is because the column with a larger slenderness ratio failed at a smaller load level, and the materials had not been fully utilised. From Figure 8, it can also be seen that a specimen fabricated from high strength concrete had a smaller ε_{cu} compared with the corresponding specimen in-filled with normal strength concrete, especially when the slenderness ratio was small. This is attributed to the fact that high-strength concrete dilates much slower under high axial loading than normal strength concrete, thus the effect of confinement from steel tube is more pronounced for the normal strength concrete. This is proved by the comparison of the lateral strains (ε_L) measured at peak loads, as shown in Table 1.

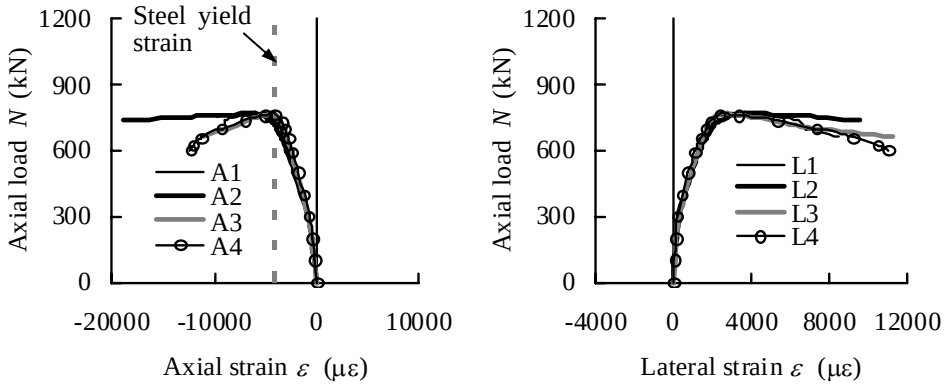

(a) S1-1a (λ=15.2, f_c'=36.3 MPa)

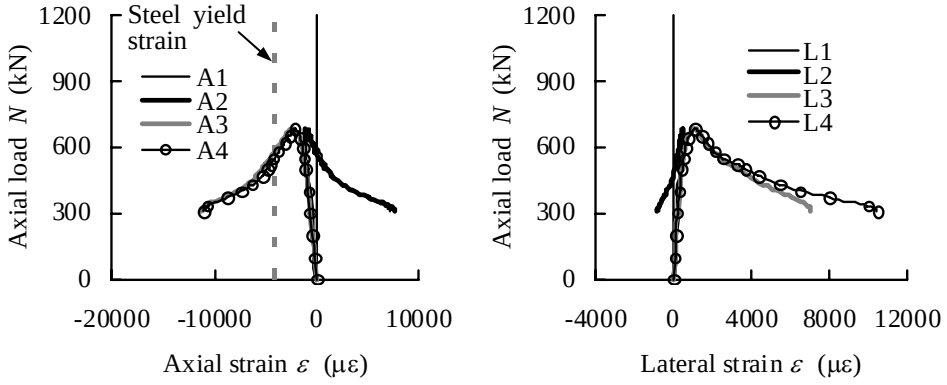

(b) S1-3b (λ=87.7, f_c'=75.4 MPa)

Figure 7. Axial and lateral strains measured at different tube locations.

Figure 9 depicts the development of the Poisson's ratios for typical steel coupon and steel tubes. The Poisson's ratios of a steel tube were calculated from strain readings with the corresponding ultimate strain shown in Table 1. To make meaningful comparison, the axial loads (N) are normalized with respect to the corresponding peak loads (N_{ue}). As far as the steel coupon is concerned, its vertical coordinate is replaced by normalized stress ($\sigma/\sigma_{0.2}$). As can be seen from Figure 9, the Poisson's ratios for all steel tubes are initially around 0.3, which are virtually the same as that of the steel coupon. Thus, the steel tubes had no confining effect on the concrete. When the load reached about 30% the peak load, the Poisson's ratio for a steel tube was bigger than that of the steel coupon. This is due to the lateral expansion of the concrete, resulting in the confinement effect from the steel tube. Therefore, it seems that the composite action between the steel tube and the concrete core still exists for slender CFSST columns, although this action decreases with increasing slenderness ratio.

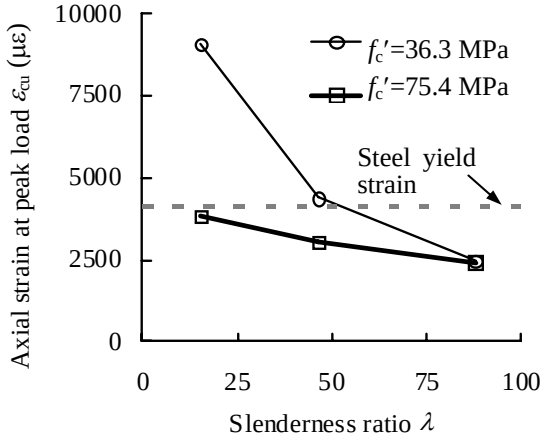

Figure 8. Effect of slenderness ratio and concrete strength on ε_{cu}.

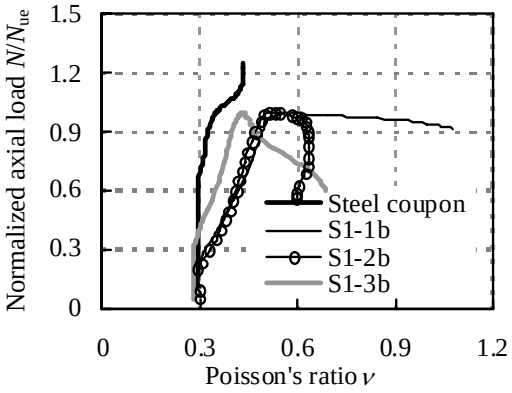

Figure 9. Development of Poisson's ratios for steel coupon and steel tubes

4 LOAD-CARRYING CAPACITY PREDICTION

Nowadays, there are several well-known national standards or recommendations to address the design of carbon steel CFST columns (Tao et al., 2008), such as Australian standard AS 5100 (Standards Australia, 2004), American code AISC (American Institute of Steel Construction, 2005), Chinese code DBJ 13-51-2003 (2003), and Eurocode 4 (2004). No standard, however, is now available for the design of CFSST columns. Based on the test results presented in this paper, the above-mentioned design codes are compared with the test results to evaluate their applicability in calculating the strength of CFSST columns. To fulfill this comparison, it should be noted that, the material partial safety factors specified in all design codes have been taken as unity when comparing code calculations with the tests. At the same time, all code limitations are ignored with a purpose to check the feasibility of those design codes in predicting the load-carrying capacities of the test specimens. The comparison between the test results N_{ue} and code predictions is shown in Table 2 and Figure 10. For simplicity reasons, the predicted results using AS 5100, AISC, DBJ and EC4 are designated as N_{AS5100}, N_{AISC}, N_{DBJ} and N_{EC4} in Table 2, respectively. The obtained average values (μ) and standard deviations (σ) are also given in Table 2. Obviously, all codes are generally conservative and underestimate the column strength by about 10-15%.

Table 2. Code predictions for CFSST columns

No.	Specimen label	N_{ue}	N_{AS5100}	N_{AS5100}/N_{ue}	N_{AISC}	N_{AISC}/N_{ue}	N_{DBJ}	N_{DBJ}/N_{ue}	N_{EC4}	N_{EC4}/N_{ue}
1	S1-1a	767.6	743.4	1.033	689.7	1.113	735.8	1.043	746.4	1.028
2	S1-1b	1090.5	1081.7	1.008	982.1	1.110	1054.6	1.034	1096.1	0.995
3	S1-2a	697.3	670.6	1.040	628.3	1.110	635.3	1.098	681.3	1.024
4	S1-2b	1022.9	942.6	1.085	874.4	1.170	833.3	1.228	964.4	1.061
5	S1-3a	622.9	481.6	1.293	479.2	1.300	488.8	1.274	488.4	1.276
6	S1-3b	684.2	627.2	1.091	623.7	1.097	600.5	1.139	586.9	1.166
μ				1.092		1.150		1.136		1.092
σ				0.104		0.078		0.098		0.108

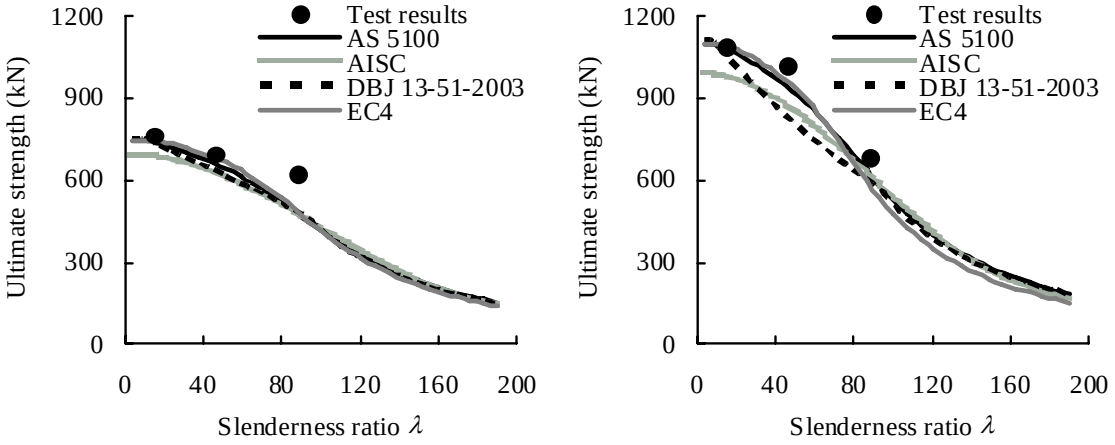

(a) Normal strength concrete (b) High strength concrete

Figure 10. Column strength based on different code predictions.

In order to further evaluate the above prediction accuracy of CFSST columns, the comparison results presented by Tao et al. (2008) for conventional rectangular carbon steel CFST columns are given in Table 3 , where a total of 234 test results was compared. It should be noted that the majority of the tests were conducted on specimens with square sections. After comparing the predictions for CFSST and carbon steel CFST columns, it can be seen that there is no significant difference in terms of prediction accuracy. However, compared with carbon steel CFST columns, all codes give a little more conservative predictions for the CFSST columns. In general, the values of μ for the CFSST columns are higher by about 2-6%.

Table 3. Comparison results of code predictions with test results of carbon steel CFST columns

AS 5100		AISC		DBJ		EC4	
μ	σ	μ	σ	μ	σ	μ	σ
1.049	0.120	1.130	0.133	1.092	0.161	1.030	0.124

5 CONCLUSIONS

Six square CFSST columns were tested under axial compression to investigate the influence of global slenderness. Comparisons of the test results were also made with several existing design methods for conventional carbon steel CFST columns. The following conclusions can be drawn within the limitation of this study:
(1) There is no obvious difference between CFSST columns and conventional carbon steel CFST columns in terms of test observation and failure modes.
(2) Composite action between steel tube and concrete core still exists for slender CFSST columns, but this action decreases with increasing slenderness ratio. Slenderness reduction factors should be applied in designing slender CFSST columns.
(3) All codes used in this paper underestimate the CFSST column strength by about 10-15%. Compared with carbon steel CFST columns, the predictions are a little more conservative.

ACKNOWLEDGEMENTS

This research work has been supported by the Research Grant Scheme and the International Research Initiatives Scheme provided by the University of Western Sydney. This support is gratefully acknowledged.

REFERENCES

ANSI/AISC 360-05. (2005). *Specification for Structural Steel Buildings*. American Institute of Steel Construction, Chicago, Illinois, USA.

DBJ 13-51-2003. (2003). *Technical Specification for Concrete-filled Steel Tubular Structures*. The Construction Department of Fujian Province, Fuzhou, China (in Chinese).

Eurocode 4. (2004). *Design of Composite Steel and Concrete Structures, Part 1.1, General Rules and Rules for Building*. BS EN 1994-1-1: 2004, British Standards Institution, London, UK.

Han, L. H. (2000). Tests on concrete filled steel tubular columns with high slenderness ratio. *Advances in Structural Engineering*, 3(4): 337-344.

Lam, D., Gardner, L. (2008). Structural design of stainless steel concrete filled columns. *Journal of Constructional Steel Research*, 64(11): 1275-1282.

Standards Australia. (2004). *Bridge Design, Part 6: Steel and Composite Construction*. AS 5100.6-2004, Sydney, Australia.

Tao, Z., Uy, B., Han, L. H., He, S. H. (2008). Design of concrete-filled steel tubular members according to the Australian Standard AS 5100 model and calibration. *Australian Journal of Structural Engineering*, 8(3): 197-214.

Uy, B. (2008). Stability and ductility of high performance steel sections with concrete infill. *Journal of Constructional Steel Research*, 64(7-8): 748-754.

Young, B., Ellobody, E. (2006). Experimental investigation of concrete-filled cold-formed high strength stainless steel tube columns. *Journal of Constructional Steel Research*, 62(5): 484-492.